Spreading of axisymmetric non-Newtonian power-law gravity currents in porous media

V. Di Federico [a,*], R. Archetti [a], S. Longo [b]

[a] Dipartimento di Ingegneria Civile, Ambientale e dei Materiali (DICAM), Università di Bologna, Italy
[b] Dipartimento di Ingegneria Civile, Ambiente Territorio e Architettura (DICATeA), Università di Parma, Italy

ABSTRACT

A relatively heavy, non-Newtonian power-law fluid of flow behavior index n is released from a point source into a saturated porous medium above an horizontal bed; the intruding volume increases with time as t^α. Spreading of the resulting axisymmetric gravity current is governed by a non-linear equation amenable to a similarity solution, yielding an asymptotic rate of spreading proportional to $t^{(\alpha+n)/(3+n)}$. The current shape factor is derived in closed-form for an instantaneous release ($\alpha = 0$), and numerically for time-dependent injection ($\alpha \neq 0$). For the general case $\alpha \neq 0$, the differential problem shows a singularity near the tip of the current and in the origin; the shape factor has an asymptote in the origin for $n \geqslant 1$ and $\alpha \neq 0$. Different kinds of analytical approximations to the general problem are developed near the origin and for the entire domain (a Frobenius series and one based on a recursive integration procedure). The behavior of the solutions is discussed for different values of n and α. The shape of the current is mostly sensitive to α and moderately to n; the case $\alpha = 3$ acts as a transition between decelerating and accelerating currents.

© 2012 Elsevier B.V. All rights reserved.

1. Introduction

Gravity currents occur when a fluid flows into another of different density; the motion, which is predominantly horizontal, is driven by gravity acting on the different densities. These currents are a common feature in many natural and artificial settings, and have been studied in the context of atmospheric sciences, geophysics, geology, reservoir engineering and hydrology; their relevance has generated a large body of literature of theoretical and experimental nature; for a review of past studies see [1–5]. A fundamental distinction is usually performed between inviscid and viscous gravity currents, depending whether the buoyancy forces are balanced by inertial or viscous forces. Gravity-driven flows in porous media are an important sub-class of viscous gravity currents, and occur when an intruding fluid is introduced or moves into natural or man-made porous formation initially saturated with another fluid. Interest in these flows is motivated by the need to model, among others, subsurface contaminant migration, saltwater intrusion, motion of lubricants around well bores, and carbon sequestration.

The literature is rich in theoretical and experimental studies that describe the spreading of single-phase Newtonian gravity currents in porous media: Huppert and Woods [6] analyzed plane flow over a horizontal impermeable surface via a similarity transformation, and performed laboratory experiments to confirm their theoretical results. Their approach was extended to axisymmetric spreading by Lyle et al. [7], and to include the effects of a permeable [8] or sloping bed [9], and of confining boundaries [10].

An extension of the aforementioned studies to flow of non-Newtonian fluids in porous media driven by density differences was undertaken recently by Di Federico et al. [11], who analyzed the motion of thin gravity currents of a power-law fluid in plane geometry, deriving a self-similar solution for the current shape under the hypothesis of a power relationship between the volume of intruding fluid and time. The solution, extending the derivations of Huppert and Woods [6] to power-law fluids, was motivated by the ubiquitous presence of rheological non-linear effects in fluids of interest in several porous media applications, such as enhanced oil recovery, propagation of contaminants in the environment, injection of remediation agents in aquifers ([11–13] and references therein) or of biomaterials in biological tissues [14,15].

In the present paper, we further extend the study of non-Newtonian gravity currents in porous media to axisymmetric spreading due to the release of a time-variable fluid volume, generalizing the approach taken earlier for Newtonian fluids in [7]. To the best of our knowledge, a similar problem was previously analyzed only by Pascal and Pascal [16] and Bataller [17], who considered an assigned injection level in the origin without introducing the volume increment of fluid with time. A consequence of

* Corresponding author.
   E-mail address: vittorio.difederico@unibo.it (V. Di Federico).

their different mathematical approach is that the special case $\alpha = 3$ separately analysed in the present paper is not individuated nor treated.

The paper is organized as follows: In Section 2, the problem is formulated in dimensionless form; the governing equations are solved via a similarity variable in Section 3; analytical and numerical results are then discussed as functions of boundary conditions and fluid flow behavior index. In Section 4, the singular behavior in the origin is discussed and approximate internal and intermediate solutions are derived. Two methods to derive an approximate analytical solution to the general problem are then presented: the first one entails the use of a Frobenius series, while the second is based on a recursive integration procedure. Finally, the special case of a quadratically increasing fluid inflow rate is examined. Conclusions are reported in Section 5.

2. Formulation

Flow of Newtonian fluids in porous media is governed by Darcy's law $\nabla P = -(\mu/k)\mathbf{u}$, implying a linear relationship between Darcy flux $\mathbf{u}$ and the gradient of the generalized pressure $P = p + \rho g z$, p being the pressure, z the vertical coordinate, μ the dynamic viscosity, and k the intrinsic permeability coefficient $[L^2]$. For non-Newtonian power-law fluids, described rheologically by the Ostwald–de Waele model, expressed in simple shear by $\tau = m\dot{\gamma}|\dot{\gamma}|^{n-1}$ (where τ is the shear stress, $\dot{\gamma}$ the shear rate, m the fluid consistency index $[ML^{-1}T^{n-2}]$ and n the flow behavior index), the modified Darcy's law takes in the literature the two equivalent forms (for a list of references see [18]).

$$\nabla P = -\frac{\mu_{eff}}{k}|\mathbf{u}|^{n-1}\mathbf{u} = -\frac{m}{k^*}|\mathbf{u}|^{n-1}\mathbf{u}, \tag{1}$$

where μ_{eff} is the effective viscosity $[ML^{-n}T^{n-2}]$ and k^* the generalized permeability $[L^{n+1}]$. The ratio $\mu_{eff}/k = m/k^*$ is termed mobility and is given by

$$\frac{k}{\mu_{eff}} = \frac{k^*}{m} = \frac{1}{2C_t}\frac{1}{m}\left(\frac{n\phi}{3+n}\right)^n\left(\frac{50k}{3\phi}\right)^{(1+n)/2}, \tag{2}$$

where ϕ denotes the porosity and $C_t = C_t(n)$ is a tortuosity factor for which different expressions are available [19].

Clearly, the two-parameter Ostwald–de Waele rheological model does not capture complex behavior involving: (i) viscoelasticity and time-dependency [20]; (ii) the rheology of Herschel–Bulkley fluids such as certain crude oils [21], which can only be approximated for vanishing values of the yield stress; (iii) the Newtonian behavior of pseudoplastic fluids at low shear rates [22]. However, the rheological behavior of many non-Newtonian fluids of interest in porous media flow is adequately represented by the power-law model for a relatively large range of shear rates or shear stresses [23], rendering it useful for engineering purposes.

The modified Darcy's law (1) and (2) was first proposed by Bird et al. [24] on the basis of a capillary bundle model of porous media; an experimental verification was provided by Cristopher and Middleman [25]; the model was later amended to include tortuosity [19].

Nonlinear filtration laws retaining the same power structure of (1) were adopted by Fadili et al. [26], Orgéas et al. [27] and Vajravelu et al. [28], and confirmed by the experiments of Yilmaz et al. [29].

Consider an infinite porous domain of depth h_0 initially saturated with an ambient fluid of density $\rho - \Delta\rho$; a thin gravity current of a non-Newtonian fluid of density ρ and height $h(r,t) \ll h_0$ is released from an axisymmetric source above an impermeable horizontal bottom (Fig. 1), so that the current volume at time t is given by $q_r t^\alpha$, with $q_r[L^3 T^{-\alpha}]$ and α being constants; the values $\alpha = 0$
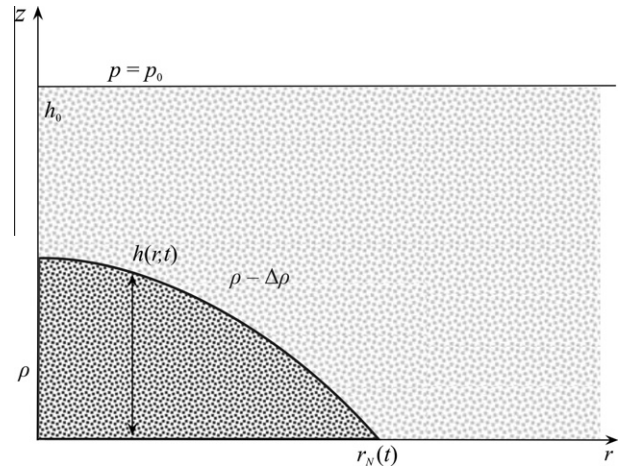

Fig. 1. Gravity current of density ρ and height $h(r,t)$ released into a porous domain saturated with fluid of density $\rho - \Delta\rho$; p_0 is the constant pressure at $z = h_0$.

(equivalent to a Dirac function as forcing term) and $\alpha = 1$ indicate respectively the instantaneous release of a fixed volume, and injection at a constant volume flux.

Considering the pressure to be hydrostatic within the intruding fluid, and neglecting mixing across the interface, secondary motions induced by the current between the two fluids, leads the filtration Eq. (1) to become

$$u(r,t) = (\Lambda\Delta\rho g)^{1/n}k^{(1+n)/(2n)}\left(-\frac{\partial h}{\partial r}\right)^{1/n}, \tag{3}$$

where

$$\Lambda = \Lambda(\phi,m,n) = \frac{1}{2C_t}\left(\frac{50}{3}\right)^{(n+1)/2}\left(\frac{n}{3n+1}\right)^n\frac{\phi^{(n-1)/2}}{m}, \tag{4}$$

while the local mass balance equation is

$$\frac{1}{r}\frac{\partial}{\partial r}(ruh) = -\phi\frac{\partial h}{\partial t}. \tag{5}$$

Substituting (3) in (5) yields

$$\frac{(\Lambda\Delta\rho g)^{1/n}k^{(1+n)/(2n)}}{\phi}\frac{1}{r}\frac{\partial}{\partial r}\left[rh\left(-\frac{\partial h}{\partial r}\right)^{1/n}\right] = -\frac{\partial h}{\partial t}. \tag{6}$$

Moreover, global continuity requires

$$2\pi\phi\int_0^{r_N(t)}rh(r,t)dr = q_r t^\alpha. \tag{7}$$

The mathematical statement of the problem is completed by the existence of a moving circular boundary of radius $r_N(t)$, where the condition $h(r \geqslant r_N(t), t) = 0$ arises for the gravity drainage flow; in the domain of integration, this reduces to:

$$h(r_N(t),t) = 0. \tag{8}$$

No physical condition can be a priori imposed on the value of the derivative at the front of the moving boundary. As discussed in [30] for the propagation of viscous gravity currents, Eq. (3) is totally incorrect at the front, and yet the solution to the governing equation can be obtained without invoking any further condition there if the Reynolds number is low (strong viscosity effects) and the Bond number is high (limited surface tension effects). In fact the condition on the spatial derivative of h at the front arises by the governing function (see Eq. (18) in Section 3). Akin to viscous gravity currents (see [30] for a detailed description) if the limits on Reynolds and/or Bond number are not satisfied, the solution should be totally controlled by the conditions at the front, that must be experimentally detected.

Introducing the dimensionless variables $T = t/t^*$, $R = r/r^*$, $R_N = r_N/r^*$, $H = h/r^*$, $U = u/V$ where the time, space and velocity scales are, for $\alpha \neq 3$, $t^* = (q_r/(\phi V^3))^{1/(3-\alpha)}$, $r^* = V \cdot t^*$, $V = (\Lambda \Delta \rho g)^{1/n} k^{(1+n)/2n}/\phi$ (Vella and Huppert [9] and Di Federico et al. [11]), recasts Eq. (8) as $H(R_N(T), T) = 0$, Eq. (3) as $U(R, T) = \phi(-\partial H/\partial R)^{1/n}$, and Eqs. (6) and (7) as

$$\frac{1}{R} \frac{\partial}{\partial R} \left[RH \left(-\frac{\partial H}{\partial R} \right)^{1/n} \right] = -\frac{\partial H}{\partial T}, \tag{9}$$

$$2\pi \int_0^{R_N(T)} RH dR = T^\alpha. \tag{10}$$

The mathematical problem constituted by Eqs. (9), (10) is solved in the sequel for $\alpha \neq 3$; for the case $\alpha = 3$, see Section 4.3.

3. Self-similar solution

To obtain a solution we consider the similarity variable

$$\eta = RT^{-\frac{\alpha+n}{3+n}}, \tag{11}$$

giving the current extension as

$$R_N(T) = \eta_N T^{(\alpha+n)/(3+n)}, \tag{12}$$

where $\eta_N = \eta_N(\alpha, n)$. Then the similarity solution of Eqs. (9) and (10) with Eq. (8) is of the form

$$H(R, T) = \eta_N^{n+1} T^{\frac{\alpha(n+1)-2n}{3+n}} \psi(\zeta), \quad \zeta = \eta/\eta_N, \tag{13}$$

with ζ being the reduced similarity variable. Substituting Eqs. (11) and (13) in Eq. (9) yields

$$\frac{d}{d\zeta} \left[\zeta \psi \left(-\frac{d\psi}{d\zeta} \right)^{1/n} \right] - \frac{n+\alpha}{3+n} \zeta^2 \frac{d\psi}{d\zeta} + \frac{\alpha(1+n) - 2n}{3+n} \zeta \psi = 0, \tag{14}$$

while Eqs. (10) and (8) transform respectively into

$$\eta_N = \left(2\pi \int_0^1 \zeta \psi(\zeta) d\zeta \right)^{-1/(3+n)}, \tag{15}$$

$$\psi(\zeta = 1) = 0. \tag{16}$$

For $n = 1$, the governing equations reduce to those derived for a Newtonian fluid in [7] in dimensional form. It follows from (11) that the velocity of the current is equal to $U = \phi \eta_N T^{(\alpha-3)/(n+3)} (-d\psi/d\zeta)^{1/n}$, i.e. the current accelerates or decelerates depending whether $\alpha > 3$ or $\alpha < 3$.

For the special case $\alpha = 0$, Eq. (14) can be integrated in closed form, yielding

$$\psi(\zeta) = \frac{n^n}{(n+1)(n+3)^n} (1 - \zeta^{n+1}) \quad \text{and}$$

$$\eta_n = \left[\pi \frac{n^n}{(n+3)^{n+1}} \right]^{-1/(n+3)}, \tag{17}$$

which reduces for $n = 1$ to Eq. (2.15) in [7]. Alternatively, integrating Eq. (14) between ζ and one yields

$$\left(-\frac{d\psi}{d\zeta} \right)^{1/n} - \frac{n+\alpha}{3+n} \zeta - \frac{\alpha}{\zeta\psi} \int_\zeta^1 \bar{\zeta}\psi d\bar{\zeta} = 0, \tag{18}$$

where the over bar indicates a dummy variable. In the limit $\alpha \to 0$ the last term is null and Eq. (18) can be directly integrated yielding for η_N the solution obtained in Pascal and Pascal [16] in dimensional form.

For arbitrary α (for the special case $\alpha = 3$, see Section 4.3) Eq. (14) can be solved numerically with (16) and a second boundary condition, which can be computed developing the asymptotic solution in terms of a Frobenius series near the current tip ($\zeta = 1$) as detailed in Appendix A, obtaining

$$\frac{d\psi}{d\zeta}\bigg|_{\zeta \to 1} = -\left(\frac{\alpha+n}{3+n} \right)^n, \tag{19}$$

thereby generalizing to a non-Newtonian fluid the behavior in the current tip of the asymptotic solution derived by Barenblatt et al. [31] and Dussan and Auzerais [32] for a Newtonian one. The numerical integration of Eq. (14) in the domain $[0, 1 - \varepsilon]$, with boundary conditions $\psi(\zeta \to 1 - \varepsilon) = ((\alpha+n)/(3+n))^n \varepsilon$ and $d\psi/d\zeta(\zeta \to 1 - \varepsilon) = ((\alpha+n)/(3+n))^n$, ε being a small quantity, is performed by using Wolfram Mathematica® 7. Results are shown as solid curves in Fig. 2, depicting the shape factor ψ for α ranging between 0 and 2 and different values of n, taken to be 0.50, 0.75 and 1.00 to cover the range most frequently encountered in practical applications with shear thinning fluids; the analysis is also performed for $n = 1.50$, to account for the rarer possibility of shear thickening fluids.

For $\alpha = 0$, the numerical solution coincides with the analytical one (black dots).

The profiles in Fig. 2 decrease as n increases for $\alpha < 1$; the reverse is true for $\alpha > 1$. For a given fluid, the shape factor increases with α, i.e. the fluid volume released into the domain.
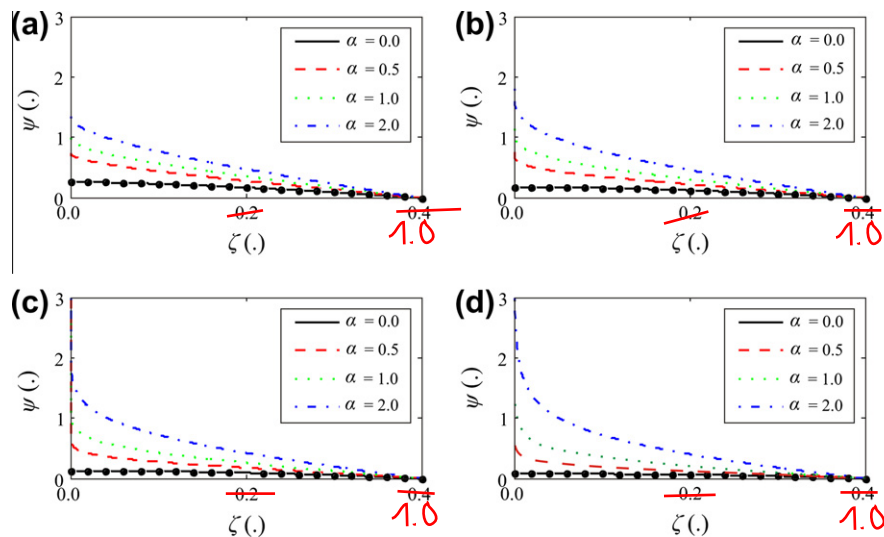

Fig. 2. Shape factor ψ versus reduced similarity variable ζ for different values of α and $n = 0.5$ (a), $n = 0.75$ (b), $n = 1.0$ (c), and $n = 1.5$ (d).
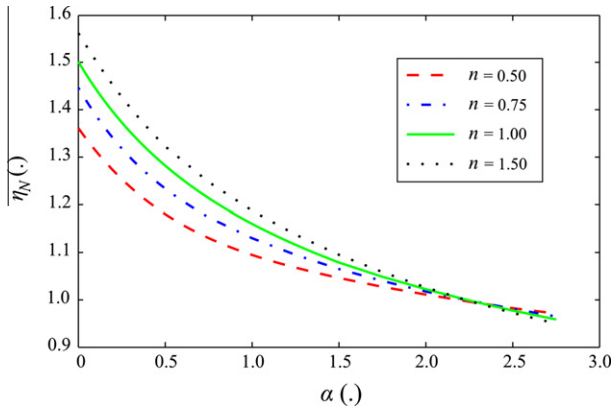
Fig. 3. The prefactor η_N versus α for different values of n.

Table 1
Ratio between current length in plane and radial geometry X_N/R_N, versus time for $\alpha = 0, 1$ and different values of n. Bold cases indicate a ratio smaller than unity.

α	0	0	0	0	1	1	1	1
T/n	0.50	0.75	1.00	1.50	0.50	0.75	1.00	1.50
0.0001	**0.86**	**0.73**	**0.64**	**0.55**	**0.28**	**0.27**	**0.28**	**0.29**
0.001	**0.99**	**0.86**	**0.78**	**0.68**	**0.41**	**0.41**	**0.41**	**0.41**
0.01	1.12	1.02	**0.94**	**0.85**	**0.61**	**0.60**	**0.60**	**0.59**
0.1	1.28	1.20	1.14	1.06	**0.91**	**0.89**	**0.87**	**0.86**
1	1.46	1.42	1.38	1.32	1.35	1.31	1.28	1.24
10	1.67	1.68	1.68	1.64	2.00	1.94	1.88	1.78
100	1.90	1.99	2.03	2.04	2.97	2.87	2.76	2.57
1000	2.17	2.35	2.46	2.54	4.41	4.24	4.06	3.70
10,000	2.47	2.78	2.98	3.17	6.54	6.27	5.95	5.33

Fig. 3 plots the multiplicative constant η_N as a function of α evaluated from the numerical solution using Eq. (15). η_N shows lower values for shear-thinning than for shear-thickening fluids when $\alpha \lesssim 2.3$; the reverse is true for $\alpha \gtrsim 2.3$; the dependence of η_N on the value of flow behavior index n is relatively modest. For a Newtonian fluid the shape factor ψ (for α ranging between 0 and 2) and the prefactor η_N perfectly reproduce the results derived by [32,7] (comparison not shown).

Once η_N is known, the current extension R_N can be evaluated from (12); for $T < 1$, the current head advances farther as n decreases; the reverse is true for $T > 1$. In Table 1, the ratio X_N/R_N between the current length in plane geometry [11], and that in radial geometry derived in the present paper, is reported versus time in the interval $T = 0.01–100$ for $\alpha = 0, 1$ and different values of n. The comparison shows that plane currents are faster than axisymmetric ones except for very short times, when the reverse is true; the value of the threshold time is a function of α and n.

Fig. 4 depicts the current evolution over time, for $\alpha = 0, 1$ $n = 0.5, 1.5$, and $T = 0.01–100$. Fig. 4a and b illustrates the release of a fixed fluid volume, showing that shear-thickening profiles are more elongated than shear-thinning ones due to their faster rate of advancement. A similar behavior is observed for constant inflow rate (Fig. 4c and d), in analogy to non-Newtonian free surface gravity currents [33].

Knowledge of the current profile and length is relevant to verify whether the injected fluid has reached a given portion of the domain; this is of interest in contamination problems and in remediation efforts.

It is worth noticing that the ratio between the current thickness and its length is given by $H/R_N = T^{(\alpha(n+1)-2n)/(\alpha+n)}$, which is a decreasing/increasing function of time respectively for $\alpha < 3$ and $\alpha \geqslant 3$; in the latter case, our solution is valid only for small times, as the assumption of a thin intruding current is eventually violated for large times.

4. Approximate solutions and special cases

In this section we discuss a number of approximate solutions to the general problem for $\alpha \neq 0$, to evidence some physical aspects of the flow field useful for further analysis. While numerical solutions are a powerful tool to solve problems intractable analytically, a close examination of related processes like flow stability preferably require, also for the sake of generality, an analytical knowledge of the basic flow, even in approximate form; the details in the degree of approximation are also necessary for the accuracy estimation of the solution.

The section closes with an analysis of the special case $\alpha = 3$ (i.e. a quadratically increasing fluid inflow rate), showing the need for an additional velocity scale.

4.1. Approximation by internal, external, and intermediate solutions

The differential Eq. (14) becomes singular in the origin because here the higher order term vanishes, as well as near the current tip if we impose there a null value of the function. While the singularity near the current tip is well managed by the Frobenius asymptotic series described in Appendix A, the behavior near the origin can be analyzed via a singular perturbation technique. Introducing an inner variable $\upsilon = \zeta/\varepsilon$, with ε a small quantity, Eq. (14) becomes

$$\frac{d}{d\upsilon}\left[\upsilon\psi\left(-\frac{d\psi}{d\upsilon}\right)^{1/n}\right] - \frac{n+\alpha}{3+n}\varepsilon^{(n+1)/n}\upsilon^2\frac{d\psi}{d\upsilon}$$
$$+ \frac{\alpha(1+n)-2n}{3+n}\varepsilon^{(n+1)/n}\upsilon\psi = 0, \tag{20}$$

Taking the limit $\varepsilon \to 0$ results in

$$\frac{d}{d\upsilon}\left[\upsilon\psi\left(-\frac{d\psi}{d\upsilon}\right)^{1/n}\right] = 0, \tag{21}$$

having solution

$$\psi = (C_1\upsilon^{(1-n)} + C_2)^{1/(n+1)} (n\neq1) \text{ and } \psi = \sqrt{C_1\ln\upsilon + C_2} (n=1), \tag{22}$$

where C_1 and C_2 are constants. The second expression in Eq. (22) was already derived by Lyle et al. [7]. For $n \geqslant 1$ the shape factor ψ grows very fast in the limit $\upsilon \to 0$, as confirmed by the numerical integration for $\alpha \neq 0$. The growth is completely balanced for $\alpha = 0$, as evident in the smooth analytical solution (17) and as shown by taking the limit of (18) for $\zeta \to 0$. Eq. (22) represents the internal solution, i.e. the approximation of the solution in a limited region near the origin. The external solution, which approximates the solution for large ζ, in theory could be computed by balancing the residual terms of order $O(\varepsilon^{1+1/n})$, but the result $\psi = C_3/x$ is incorrect since it cannot satisfy the boundary condition at the current tip. Hence we choose to assume the external solution equal to the Frobenius series near the current tip (see Appendix A). The two functions are

$$\psi_{int} = \left[C_1\left(\frac{\zeta}{\varepsilon}\right)^{(1-n)}\right]^{1/(n+1)}, \quad n\neq1, \quad \varepsilon \to 0^+, \quad \zeta \to 0^+, \tag{23}$$

$$\psi_{ext} = a_0(1-\zeta) + a_1(1-\zeta)^2 + a_2(1-\zeta)^3 + O(\zeta^4), \tag{24}$$

where the second constant C_2 in the internal solution has been fixed equal to zero. The first constant is computed by imposing the matching condition $\lim_{\varepsilon\to0^+,\zeta\to0^+}\psi_{int} = \lim_{\zeta\to0^+}\psi_{ext}$, yielding

$$\psi_{int} = \left(\sum_{k=0}^{2}a_k\right)\zeta^{(1-n)/(1+n)}. \tag{25}$$
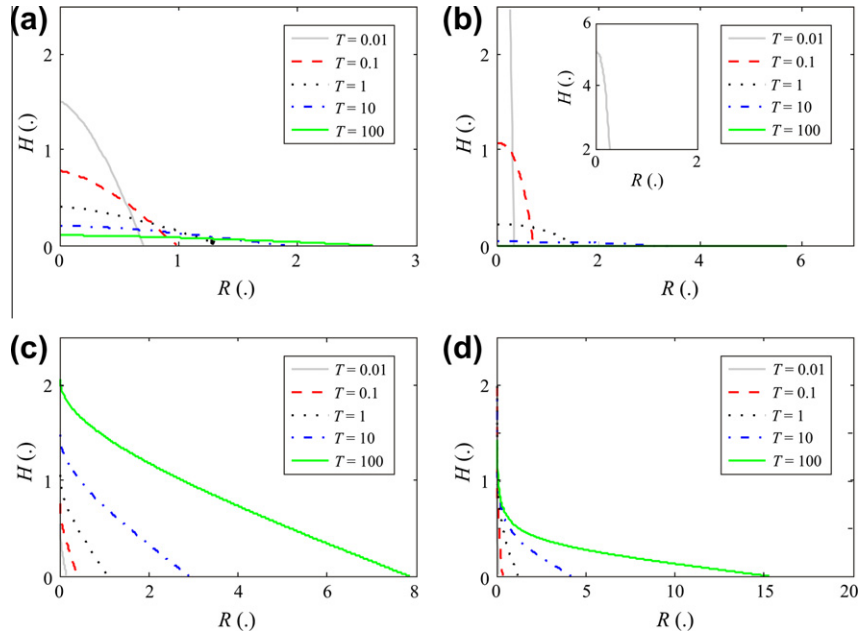
Fig. 4. Profiles of the current at different times for (a) $\alpha = 0$ and $n = 0.5$; (b), as (a) but $n = 1.5$; (c) $\alpha = 1$ and $n = 0.5$; and (d) as (c) but $n = 1.5$.

Eq. (25) reveals that the origin is an asymptote only for the case $n > 1$. Since the profiles show that for $\alpha = 0$ no singularity develops near the origin, a dependence of the coefficient C_1 on α is expected. An intermediate limit analysis reveals that this conjecture is true. Performing the expansion in an inner variable of Eq. (18) gives

$$\left(-\frac{d\psi}{d\upsilon}\right)^{1/n} - \frac{n+\alpha}{3+n}\varepsilon^{n+1}\upsilon - \frac{\alpha}{\upsilon\psi}\varepsilon^{n-1}\left(\int_0^1 \bar{\zeta}\psi d\bar{\zeta} - \int_0^{\varepsilon\upsilon} \varepsilon^2 \bar{\upsilon}\psi d\bar{\upsilon}\right) = 0. \tag{26}$$

Note that the integral contribution has been split in a finite order term plus a residual contribution which is at least of order $O(\varepsilon^{n+5})$. Hence the two main terms to balance are

$$\left(-\frac{d\psi}{d\upsilon}\right)^{1/n} - \frac{\alpha}{\upsilon\psi}\varepsilon^{n-1}\left(\int_0^1 \bar{\zeta}\psi d\bar{\zeta}\right) = 0 \qquad \text{for } \upsilon \to 0, \quad n \neq 1. \tag{27}$$

Integration results in the intermediate solution

$$\psi_{imd} = \varepsilon^{n(n-1)/(n+1)}\left[\frac{n+1}{1-n}\alpha^n\left(\int_0^1 \bar{\zeta}\psi d\bar{\zeta}\right)^n (1-\upsilon^{1-n})\right]^{1/(n+1)} \tag{28}$$

As long as $\varepsilon^{n(n-1)/(n+1)}$ is of finite order in the intermediate limit of small ζ, Eq. (28) is a better approximation than Eq. (22). No asymptote is expected for $n > 1$ or for $\alpha = 0$. The integral can be evaluated by using the external solution in Frobenius series, which gives an excellent approximation of the true shape factor.

A plot of the internal, of the external and of the intermediate functions versus the reduced similarity variable is shown for $n = 2$, $\alpha = 2$ in Fig. 5, in which the horizontal axis has a square root distortion for a more detailed representation of the internal region. The internal and intermediate functions are given by (25) and (28) respectively, while the external solution is a Frobenius series with four terms. The relative error is shown in the upper Figure panel. Note that the intermediate solution is almost coincident with the numerical solution near the origin and is a better approximation than the inner solution, while the internal solution has an error exceeding the displayed range. The introduction of a matching function between the intermediate and the external solutions is potentially meaningful only in a small interval near $\zeta \approx 0.3$.

In conclusion, the rapid growth and the asymptotic behavior of the shape function near the origin can be mathematically handled;
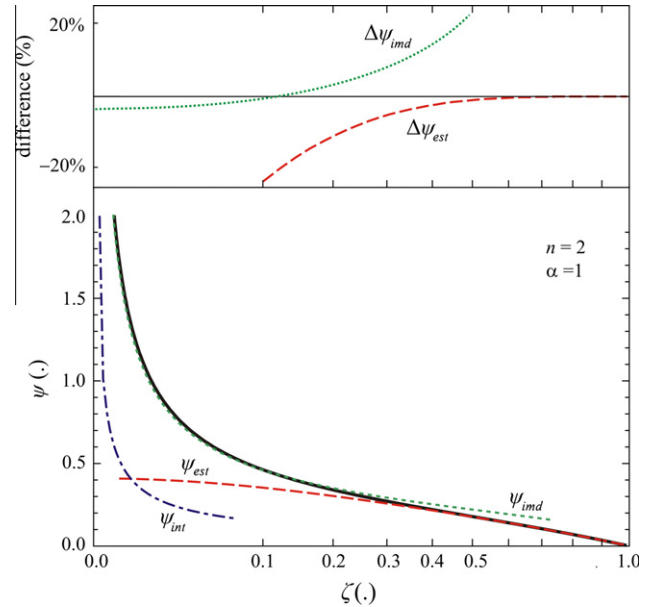

Fig. 5. Approximation of the shape function (bold curve) through the internal solution (dot-dashed curve), the external solution (dashed curve), and the intermediate solution (dotted curve), for $n = 2$, $\alpha = 2$.

nevertheless we highlight that such behavior of the shape function invalidates the hypotheses of the model, being a violation of the small-slope approximation in the adopted theory. A reasonable practical approach is to exclude from the computation a small cylinder with $\zeta < \zeta_0$ containing a negligible volume of fluid compared to $q_r t^\alpha$. This does not influence the solution which is obtained integrating from the front end of the current.

4.2. Approximate solutions in series and by iterative integration

In the following we briefly consider and discuss two different methods to obtain an approximate solution valid for any value of α and n. Even though a numerical solution can be easily computed with high accuracy, analytical or semianalytical solutions are

better suited whenever it is necessary to evaluate the relative importance of the different terms in the balance equation, or for extracting the behavior of a variable, like the dependence of the position of the front edge on the parameter α. The first one, presented in the Appendix A and already adopted in [11], entails the use of a Frobenius series, and allows derivation of an approximate solution for the shape factor given by Eq. (A.1). Since shear thinning fluids do not show a singularity in the origin, the Frobenius series is an excellent expansion in the entire domain; the adoption of a few terms of the series implies a very limited error in the shape factor and an even smaller error in the current length, which is fairly uniform with the parameter α, as shown by Fig. 6, which illustrates the prefactor η_N (a proxy for current length) versus α for a shear thinning fluid with $n = 0.5$, demonstrating that the two curves obtained numerically (bold line) and with a Frobenius series of four terms exhibit a difference less than 2%.

The shear thickening fluids require an alternative approach based on an iterative integration of Eq. (18) with an approximation of the integral term, generalizing the comprehensive one developed for Newtonian fluids by Li et al. [34] and also applied to plane gravity currents [11]. The approach is detailed in Appendix B.

The convergence of the latter solution is very fast, as shown in Fig. 7 for the case $n = 2$, $\alpha = 1$, where a single iteration gives a marked improvement over the starting solution ψ_0 and a good agreement with the numerical one. The final approximation is of order α^{nr} with a better approximation for smaller values of α. The drawback of the method illustrated in Appendix B is the difficulty to solve analytically the integrals that contain numerous terms.

Fig. 8 shows the comparison between the values of the prefactor η_N obtained by direct numerical integration and the approximate method of Appendix B. The error is quite limited even for larger values of exponent α. Similar results are obtained for different values of the flow behavior index if $n > 1$, even though the error grows with n. In the same figure, the results obtained with a Frobenius series are shown for comparison, demonstrating an even better approximation despite the fact that the Frobenius series loses validity near the origin, where a singularity is expected for $\alpha \neq 0$. Note that the error in evaluating η_N is smaller than the corresponding error in the shape factor, because the larger errors in the approximation of the shape factor are for $\zeta \to 0$, i.e. in a region which gives a small contribution to the integral in Eq. (B.1) and which can be safely excluded from the computation since its contribution to the total volume of fluid is negligible.

4.3. The special case $\alpha = 3$

When $\alpha = 3$ the characteristic time scale t^* introduced in Section 2 is no longer defined, and an additional natural velocity scale
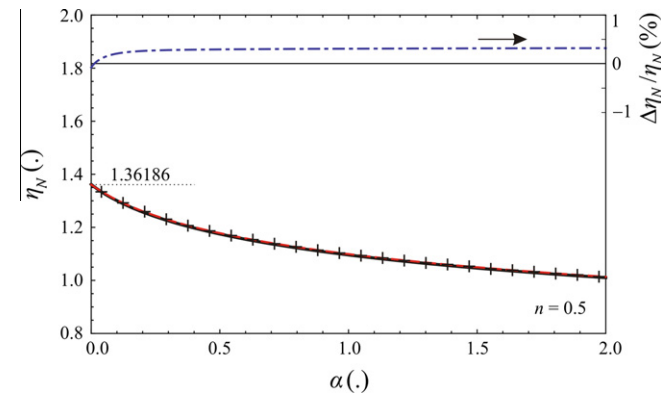

Fig. 6. Values of η_N versus α for a shear thinning fluid with $n = 0.5$ obtained numerically (bold line) and with a Frobenius series of four terms (see Appendix A) (dashed line plus crosses). The dashdot curve is the relative error.
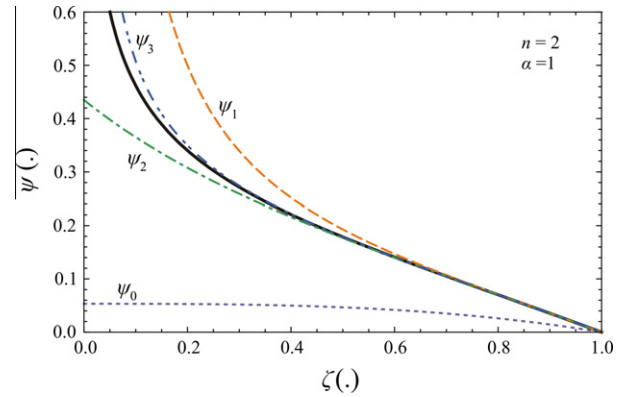

Fig. 7. Shape factor ψ versus ζ obtained numerically and quasi-analytically with the integration by approximation for shear-thickening fluid with $n = 2$ and $\alpha = 1$. The bold curve is the numerical result, the dotted line the analytical solution ψ_0 (17), the dashed line is the first iteration ψ_1 and so on.
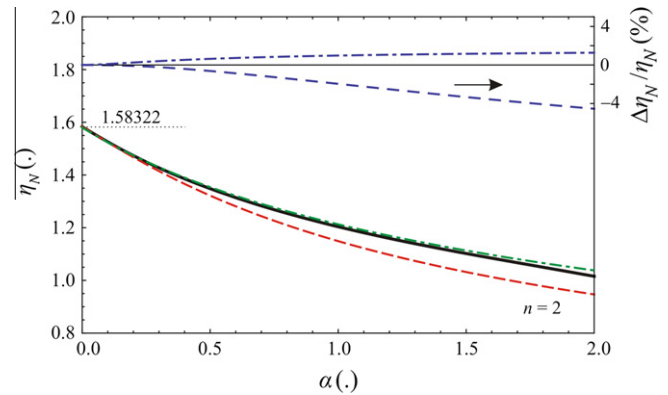

Fig. 8. Values of η_N versus α for a shear-thickening fluid with $n = 2$ obtained numerically (bold line), with Eq. (B.4) (dashed line) and with a Frobenius series with four terms (dashdot line). The upper insert shows the relative error.

$(q_r/\phi)^{1/3}$ enters the problem. A new set of dimensionless variables is thus defined in analogy to [9] as $\widetilde{R} = r/\tilde{r}^*$, $\widetilde{R}_N = r_N/\tilde{r}^*$, $\widetilde{H} = h/\tilde{r}^*$, where $\tilde{r}^* = (q_r/\phi)^{1/3}\tilde{t}^*$ is a spatial length scale and $\tilde{t}^*$ an arbitrary time scale. Eqs. (9) and (10) are then re-cast as

$$\frac{\delta_r}{\widetilde{R}}\frac{\partial}{\partial\widetilde{R}}\left[\widetilde{R}\widetilde{H}\left(-\frac{\partial\widetilde{H}}{\partial\widetilde{R}}\right)^{1/n}\right] = -\frac{\partial\widetilde{H}}{\partial\widetilde{T}}, \tag{29}$$

$$2\pi\phi\int_0^{\widetilde{R}_N(\widetilde{T})}\widetilde{R}\widetilde{H}d\widetilde{R} = \widetilde{T}^3, \tag{30}$$

where $\delta_r = V/(q_r/\varphi)^{1/3}$ is the ratio between the two velocity scales in the problem. Here, the similarity variable (12) reduces to $\eta = \widetilde{R}/\widetilde{T}$; in analogy to the general case, the current height is given by $\widetilde{H}(\widetilde{R}, \widetilde{T}) = \eta_N^{n+1}T\psi(\eta/\eta_N)$, where the shape factor ψ is derived by solving

positive sign

$$\delta_r\frac{d}{d\zeta}\left[\zeta\psi\left(-\frac{d\psi}{d\zeta}\right)^{1/n}\right] - \zeta^2\frac{d\psi}{d\zeta} + \zeta\psi = 0. \tag{31}$$

Since no analytical solution is available for Eq. (31), a numerical integration is required; the boundary conditions are derived by means of the same procedure adopted for the general case (see Eq. (A.8)). The results of this calculation are shown in Fig. 9 for different values of δ_r and two values of n. An increase in δ_r produces a
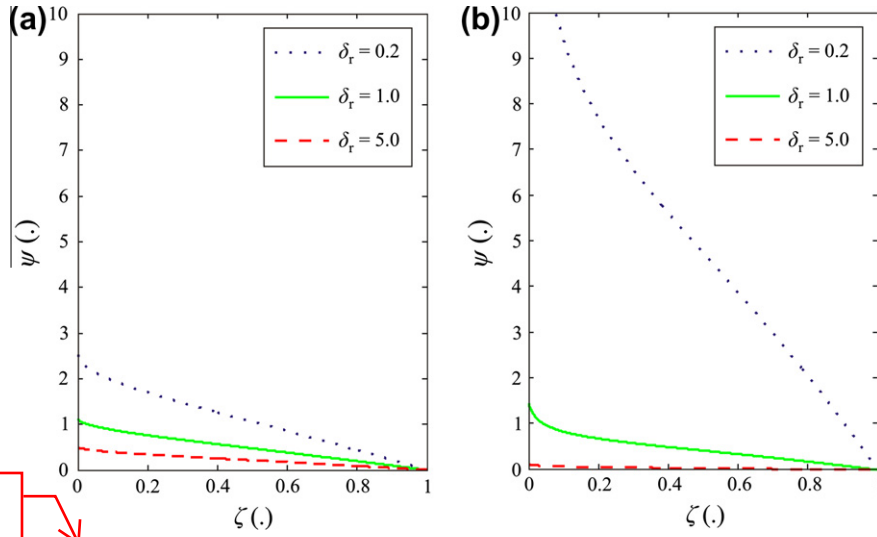
Fig. 9. Shape factor for $\alpha = 3$ and $\delta_r = 0.2, 1.0, 5.0$ with (a) $n = 0.50$ and (b) $n = 1.50$.

the plots refer to the wrong sign in eq. 31

decrease in the shape factor and vice versa; the impact of the actual value of δ_r is larger for shear-thickening than for shear-thinning fluids.

5. Conclusions

The following conclusions may be derived from our study of the horizontal axisymmetric spreading of non-Newtonian power-law gravity currents in a porous layer initially saturated with an ambient fluid of lower density:

1. The set of non-linear differential equations governing the spreading admits a relatively simple similarity solution, which is derived in closed-form for the release of a fixed volume of fluid, and numerically for time-dependent inflow. For a Newtonian fluid, the formulation and solution reduce to those obtained earlier in [7].
2. The solution: (a) has no undetermined parameters, since the motion of the external ambient fluid is neglected; (b) is completely independent on the details near the current tip, since the boundary conditions derive from an analysis of the differential equation; and (c) is globally insensitive to front effects for low Reynolds number and high Bond number.
3. The shape factors: (a) have an infinite slope in the origin for shear-thickening fluids and a continuous inflow; for an instantaneous release or shear-thinning fluids, no asymptote is present; (b) exhibit a finite slope at the current tip, decreasing with increasing flow behavior index, in variance with free-surface flows; (c) depend strongly upon the release rate and moderately upon the value of flow behavior index; (d) if an asymptote is present, may be approximated near the origin by an intermediate solution considering only the leading terms; and (e) if no asymptote is present, may be approximated in the whole domain by a Frobenius series (see next point).
4. Two approximate analytical solutions are derived to complement the numerical results. The first entails the use of a Frobenius series, and provides a power formulation of the shape factor near the current tip; for shear-thinning fluids, not showing a singularity in the origin, the solution is acceptable in the entire domain; the computation of the coefficients is in principle extendible to any order adopting customary

symbolic software. The second approximation, valid for both shear-thickening and shear-thinning fluids, is based upon a series expansion in the exponent governing the current volume increase with time, followed by an integration by iteration; it provides a fairly accurate solution in the entire domain, but analytical integration soon becomes too cumbersome.
5. Our result, despite model simplifications, provide insight into non-Newtonian effects on flow of gravity currents in porous media by means of closed-form results with which the sensitivity of results to different parameters may be tested. The prediction of the current profile and length for instantaneous and continuous injection are relevant in contamination problems and remediation efforts.

Appendix A. Derivation of an asymptotic solution near the current tip ($\zeta = 1$)

Here we wish to derive a series expansion of the shape factor being the solution of the differential problem given by Eq. (14) with $\alpha \neq 3$, subject to the boundary condition $\psi(\zeta \to 1) = 0$. The derivation has the additional aim of deriving a second boundary condition in $\zeta = 1$, suitable for numerical integration. Introducing the variable $\chi = 1 - \zeta$, we seek a solution as $\chi \to 0$ in the form of a Frobenius series with indicial exponent b

$$\psi(\chi) = \sum_0^\infty a_k \chi^{k+b}, \tag{A.1}$$

already fulfilling the boundary condition $\psi(\chi \to 0) = 0$. Deriving its derivative and $1/n$th power (for explicit expressions see [11]) and substituting in (14) leads to

$$-a_0^{\frac{n+1}{n}} b^{\frac{1}{n}} \left(\frac{b-1}{n} + b \right) \chi^{\frac{b-1}{n}+b-1} - a_1 a_0^{\frac{1}{n}} b^{\frac{1}{n}} \left(\frac{b-1}{n} + b + 1 \right) \chi^{\frac{b-1}{n}+b} + \cdots$$

$$+ \frac{\alpha+n}{3+n} \sum_0^\infty a_k (b+k) \chi^{b+k-1} - \frac{\alpha+n}{3+n} \sum_0^\infty a_k (b+k) \chi^{b+k+1}$$

$$+ \frac{\alpha(n+1)-2n}{3+n} \sum_0^\infty a_k \chi^{b+k} - \frac{\alpha(n+1)-2n}{3+n} \sum_0^\infty a_k \chi^{b+k+1} = 0, \tag{A.2}$$

Equating the lowest powers of χ (for $k = 0$) gives $b = 1$, while equating the coefficients of powers of χ (for $k > 0$) to zero yields

$$a_0 = f^n, \tag{A.3a}$$

$$a_1 = \frac{a_0 n(g - 2f + 2a_0^{1/n})}{2(2+n)a_0^{1/n} - 2fn}, \tag{A.3b}$$

$$a_2 = \frac{a_0 n^2(g-f) - a_1 n^2(g-4f) - 3a_0^{1/n} a_1 n(2+n) + 6a_0^{1/n-1} a_1^2}{3n[nf - a_0^{1/n}(3+n)]}, \tag{A.3c}$$

with

$$f = \frac{\alpha+n}{3+n}; \quad g = \frac{\alpha(n+1) - 2n}{3+n}, \tag{A.4a, b}$$

Hence the second-order asymptotic solution is

$$\psi(\zeta) = \left(\frac{\alpha+n}{3+n}\right)^n (1-\zeta) + O(\zeta^2); \tag{A.5}$$

its first derivative evaluated at $\zeta = 1$ is then easily derived as Eq. (19). For $\alpha = 0$, the boundary condition satisfies the analytical solution in Eq. (17).

We next discuss the special case $\alpha = 3$, governed by Eq. (31) subject to $\psi(\zeta \to 1) = 0$. Following the approach adopted for the general case, we again find the indicial exponent to be 1; hence the Frobenius series takes the form

$$\psi(1-\zeta) \equiv \sum_0^\infty a_k (1-\zeta)^{k+b}, \tag{A.6}$$

in which the first three coefficients are given by

$$a_0 = \left(\frac{1}{\delta_r}\right)^n, \tag{A.7a}$$

$$a_1 = \frac{a_0 n(2\delta_r a_0^{1/n} - 3)}{2(2+n)\delta_r a_0^{1/n} - 2n}, \tag{A.7b}$$

$$a_2 = \frac{2a_0 n^2 - 5a_1 n^2 + 3\delta_r n a_0^{1/n} a_1(2+n) - 6\delta_r a_0^{1/n-1} a_1^2}{3n[\delta_r a_0^{1/n}(3+1) - n]}. \tag{A.7c}$$

Hence at first order

$$\frac{d\psi}{d\zeta} = -\left(\frac{1}{\delta_r}\right)^n + O(\zeta). \tag{A.8}$$

Appendix B. Derivation of the approximate solution by iterative integration

In order to obtain an approximation of the shape factor, we consider a series expansion of Eq. (14) for small α, followed by an integration by iteration of Eq. (18) with

$$\frac{d\psi_1}{d\zeta} = -\left(\frac{n+\alpha}{3+n}\zeta + \frac{\alpha}{\zeta\psi_0}\int_\zeta^1 \zeta\psi_0 d\zeta\right)^n$$

$$\frac{d\psi_2}{d\zeta} = -\left(\frac{n+\alpha}{3+n}\zeta + \frac{\alpha}{\zeta\psi_1}\int_\zeta^1 \zeta\psi_1 d\zeta\right)^n$$

$$\cdots \tag{B.1}$$

$$\frac{d\psi_r}{d\zeta} = -\left(\frac{n+\alpha}{3+n}\zeta + \frac{\alpha}{\zeta\psi_{r-1}}\int_\zeta^1 \zeta\psi_{r-1} d\zeta\right)^n,$$

where ψ_0 is the starting solution coincident with the analytical solution for $\alpha = 0$ (Eq. (17)), ψ_1 is the is the solution after the first iteration, and so on.

Some indications on the leading terms behavior can be detected analyzing the structure of the differential problem. For simplicity of computation we will focus the analysis on fluids with $n = 2$. In this case the first iteration in Eq. (B.1) gives the following approximation

$$\psi_1 = \frac{4}{75}(1 - \zeta^3)$$
$$+ \frac{1}{75}\alpha\left[4\pi\sqrt{3} - 6\sqrt{3}\tan^{-1}\left(\frac{1+2\zeta}{\sqrt{3}}\right) + 9\ln\left(\frac{3}{1+\zeta+\zeta^2}\right)\right]$$
$$+ \frac{1}{300}\alpha^2\left[\frac{27}{\zeta} + 9\frac{\zeta-1}{1+\zeta+\zeta^2} + 24\sqrt{3}\tan^{-1}\left(\frac{1+2\zeta}{\sqrt{3}}\right) - 8\pi\sqrt{3} - 27\right], \tag{B.2}$$

which introduces a fast growing term $\approx 1/\zeta$ in the quadratic contribution α^2. As the first moment of the approximate shape factor given by Eq. (B.2) is equal to

$$\int_0^1 \zeta\psi_1 d\zeta = \frac{2}{125} + \frac{1}{150}\alpha(9 + \pi\sqrt{3} - 9\ln 3) + \frac{1}{600}\alpha^2(9 + 2\pi\sqrt{3}) + O(\alpha^3), \tag{B.3}$$

the factor η_N can be obtained using Eq. (15) as

$$\eta_N = \left(2\pi\left[\frac{2}{125} + \frac{1}{150}\alpha(9 + \pi\sqrt{3} - 9\ln 3) + \frac{1}{600}\alpha^2(9 + 2\pi\sqrt{3})\right]\right)^{-1/5}. \tag{B.4}$$

For a generic value of n, the contribution of the first order approximation in the limit $\zeta \to 0$ shows that if $n < 1$ no singularity is expected in the origin.

References

[1] H.E. Huppert, The intrusion of fluid mechanics into geology, J. Fluid Mech. 173 (1986) 557–598.
[2] H.E. Huppert, Gravity currents: a personal perspective, J. Fluid Mech. 554 (2006) 299–322.
[3] J.E. Simpson, Gravity currents in the laboratory, atmosphere, and ocean, Ann. Rev. Fl. Mech. 14 (1982) 213–234.
[4] J.E. Simpson, Gravity Currents: In the Environment and the Laboratory, second ed., Cambridge University Press, Cambridge, 1997.
[5] M. Ungarish, An Introduction to Gravity Currents and Intrusions, CRC Press, Boca Raton, 2010.
[6] H.E. Huppert, A.W. Woods, Gravity-driven flows in porous layers, J. Fluid Mech. 292 (1995) 55–69.
[7] S. Lyle, H.E. Huppert, M. Hallworth, M. Bickle, A. Chadwick, Axisymmetric gravity currents in a porous medium, J. Fluid Mech. 543 (2005) 293–302.
[8] D. Pritchard, A.W. Woods, A.J. Hogg, On the slow draining of a gravity current moving through a layered permeable medium, J. Fluid Mech. 444 (2001) 23–47.
[9] D. Vella, H.E. Huppert, Gravity currents in a porous medium at an inclined plane, J. Fluid Mech. 555 (2006) 353–362.
[10] M.J. Golding, H.E. Huppert, The effect of confining impermeable boundaries on gravity currents in a porous medium, J. Fluid Mech. 649 (2010) 1–17.
[11] V. Di Federico, R. Archetti, S. Longo, Similarity solutions for spreading of a two-dimensional non-Newtonian gravity current in a porous layer, J. Non-Newton. Fluid Mech. 177–178 (2012) 46–53, http://dx.doi.org/10.1016/j.jnnfm.2012.04.003.
[12] V. Di Federico, V. Ciriello, Generalized Solution for 1-D non-Newtonian flow in a porous domain due to an instantaneous mass injection, Transp. Por. Med. 93 (2012) 63–77, http://dx.doi.org/10.1007/s11242-012-9944-9.
[13] V. Ciriello, V. Di Federico, Similarity solutions for flow of non-Newtonian fluids in porous media revisited under parameter uncertainty, Adv. Wat. Res. 43 (2012) 38–51, http://dx.doi.org/10.1016/j.advwatres.2012.03.028.
[14] G. Baroud, M. Crookshank, M. Bonner, High-viscosity cement significantly enhances uniformity of cement filling in vertebroplasty: an experimental model and study on cement leakage, SPINE 31 (22) (2006) 2562–2568.
[15] G.A. Ateshian, The role of interstitial fluid pressurization in articular cartilage lubrication, J. Biomech. 42 (9) (2009) 1163–1176.
[16] J.P. Pascal, H. Pascal, Similarity solutions to gravity flows of non-Newtonian fluids through porous media, Int. J. Non-Linear Mech. 28 (2) (1993) 157–167.
[17] R.C. Bataller, On unsteady gravity flows of a power-law fluid through a porous medium, Appl. Math. Comput. 196 (2008) 356–362.
[18] V. Di Federico, M. Pinelli, R. Ugarelli, Estimates of effective permeability for non-Newtonian fluid flow in randomly heterogeneous porous media, Stoch. Environ. Res. Risk Assess. 24 (7) (2010) 1067–1076, http://dx.doi.org/10.1007/s00477-010-0397-9.
[19] A.V. Shenoy, Non-Newtonian fluid heat transfer in porous media, Adv. Heat Trans. 24 (1995) 102–190.
[20] T. Sochi, Newtonian flow in porous media, Polymer 51 (2010) 5007–5023.
[21] S. Wang, Y. Huang, F. Civan, Experimental and theoretical investigation of the Zaoyuan field heavy oil flow through porous media, J. Pet. Sci. Eng. 50 (2006) 83–101.
[22] Y.-S. Wu, K. Pruess, Flow of non-Newtonian fluids in porous media, Adv. Por. Med. 3 (1996) 87–184.

[23] M.T. Ghannam, W. Shadi, S.W. Hasan, B. Abu-Jdayil, N. Esmail, Rheological properties of heavy & light crude oil mixtures for improving flowability, J. Petrol. Sci. Eng. 81 (2012) 122–128.

[24] R.B. Bird, W.E. Stewart, E.N. Lightfoot, Transport Phenomena, Wiley, 1960.

[25] R.H. Cristopher, S. Middleman, Power-law flow through a packed tube, Ind. Eng. Chem. Fundam. 4 (4) (1965) 422–427.

[26] A. Fadili, P.M.J. Tardy, A. Pearson, A 3D filtration law for power-law fluids in heterogeneous porous media, J. Non-Newton. Fluid Mech. 106 (2002) 121–146.

[27] L. Orgéas, Z. Idrisa, C. Geindreaua, J.F. Blochb, J.L. Auriault, Modelling the flow of power-law fluids through anisotropic porous media at low-pore Reynolds number, Chem. Eng. Sci. 61 (2006) 4490–4502.

[28] K. Vajravelu, S. Sreenadh, G. Viswanatha Reddy, Helical flow of a power-law fluid in a thin annulus with permeable walls, Int. J. Non-Linear Mech. 41 (2006) 761–765.

[29] N. Yilmaz, A.S. Bakhtiyarov, R.N. Ibragimov, Experimental investigation of Newtonian and non-Newtonian fluid flows in porous media, Mech. Res. Commun. 36 (5) (2009) 638–641.

[30] H.E. Huppert, The propagation of two-dimensional and axisymmetric viscous gravity currents over a rigid horizontal surface, J. Fluid Mech. 121 (1982) 43–58.

[31] G.I. Barenblatt, V.M. Entov, V.M. Ryzhik, Theory of Fluid Flows Through Natural Rocks, Kluwer Academic Publishers, Dordrecht, 1990.

[32] E.B. Dussan V, F.M. Auzerais, Buoyancy-induced flow in porous media generated near a drilled oil well. Part 1. The accumulation of filtrate at an horizontal impermeable boundary, J. Fluid Mech. 254 (1993) 283–311.

[33] V. Di Federico, S. Cintoli, S. Malavasi, Viscous spreading of non-Newtonian gravity currents on a plane, Meccanica 41 (2) (2006) 207–217.

[34] L. Li, D.A. Lockington, M.B. Parlange, F. Stagnitti, D.S. Jeng, J.S. Selker, A.S. Telyakovskiy, D.A. Barry, J.Y. Parlange, Similarity solution of axisymmetric flow in porous media, Adv. Wat. Res. 28 (2005) 1076–1082.

ERRATA-CORRIGE

In this paper eq. 2 p.32 is erratum

$$\frac{k}{\mu_{eff}} = \frac{k^*}{m} = \frac{1}{2C_t}\frac{1}{m}\left(\frac{n\phi}{3+n}\right)^n\left(\frac{50k}{3\phi}\right)^{(1+n)/2},$$

(2)

...

The rectification is:

$$\frac{k}{\mu_{eff}} = \frac{k^*}{m} = \frac{1}{2C_t}\frac{1}{m}\left(\frac{n\phi}{3n+1}\right)^n\left(\frac{50k}{3\phi}\right)^{(1+n)/2},$$

(2)

...

Eq. 17, p.33 is erratum:

$$\psi(\zeta) = \frac{n^n}{(n+1)(n+3)^n}\left(1-\zeta^{n+1}\right) \text{ and}$$

(17)

$$g_n = \left[\pi\frac{n^n}{(n+3)^{n+1}}\right]^{-1/(n+3)},$$
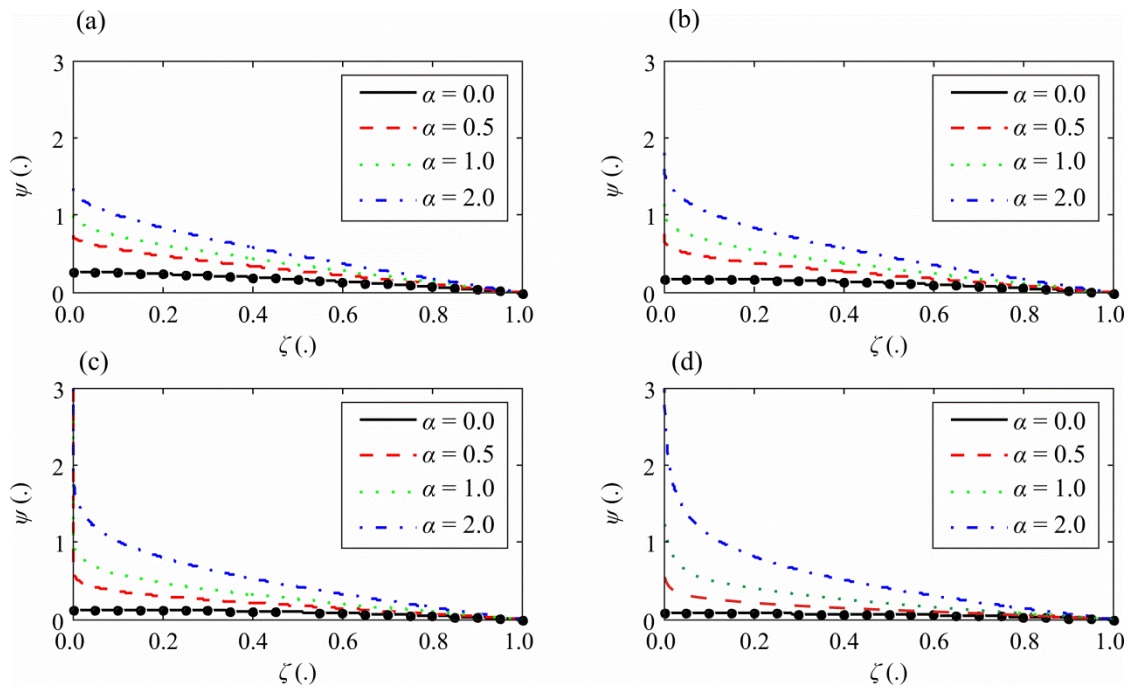
...

The rectification is:

$$\psi(\zeta) = \frac{n^n}{(n+1)(n+3)^n}\left(1-\zeta^{n+1}\right) \text{ and}$$

(17)

$$\eta_N = \left[\pi\frac{n^n}{(n+3)^{n+1}}\right]^{-1/(n+3)},$$

In Fig.2 p.33 the limits of the horizontal axis in the figure are wrong. In facts the limits are 0-0.4 but should be 0-1.0. The corrected Figure is below:

Last term of eq. 31: change sign from - to +
Plots in Figure 9: refer to the wrong sign of eq. 31